Advances in Nano Research, *Vol. 12, No. 5 (2022) 457-465*
https://doi.org/10.12989/anr.2022.12.5.457

Separation of cadmium and chromium heavy metals from industrial wastewater by using Ni-Zn nanoferrites

Atul Thakur*[1], Pinki Punia[2], Rakesh Dhar[2], R. K. Aggarwal[3] and Preeti Thakur**[4]

[1]*Amity Institute of Nanotechnology, Amity University Haryana, Gurugram, Haryana 122413, India*
[2]*Department of Physics, Guru Jambheshwar University of Science & Technology, Hisar, Haryana 125001, India*
[3]*Department of Environmental Science, Dr. Y. S. Parmar University, Nauni, Solan 173230 HP, India*
[4]*Department of Physics, Amity University Haryana, Gurugram, Haryana 122413, India*

(*Received November 15, 2021, Revised February 13, 2022, Accepted February 13, 2022*)

Abstract. The potentials of $Ni_xZn_{1-x}Fe_2O_4$ (x = 0.0, 0.2, 0.4, 0.6, 0.8 and 1.0) nanoadsorbents were investigated for removal of Cd and Cr from contaminated water from an electroplating industry in Himachal Pradesh, India. Optimal values were recorded under batch adsorption experiments performed to remove dissolved heavy metal ions from industrial wastewater. The specific surface area (*SSA*) of nanoadsorbents perceived to vary in a range 35.75-45.29 cm^2/g and was calculated from the XRD data. The influence of two operating parameters, contact time and dopant (Ni) concentration was also investigated at pH ~7 with optimum dosage. Kinetic studies were conducted within a time range of 2-10 min with rapid adsorption of cadmium and chromium ions onto $Ni_{0.2}Zn_{0.8}Fe_2O_4$ nanoadsorbents. Pseudo-second-order kinetic model was observed to be well fitted with the adsorption data that confirmed the only existence of chemisorption throughout the adsorption process. The maximum adsorption efficiency values observed for Cd and Cr were 51.4 mg/g and 40.12 mg/g, respectively for different compositions of prepared series of nanoadsorbents. The removal percentage of Cd and Cr was found to vary in a range of 47.7%-95.25% and 21%-50% respectively. The prepared series of nanoferrite found to be suitable enough for adsorption of both heavy metal ions.
Keywords: adsorption efficiency; adsorption kinetics; heavy metals; industrial wastewater; nanoadsorbents

1. Introduction

Heavy metals are the key contaminants in industrial waste water among all other organic, inorganic and microbial pollutants. Various toxic heavy metals are present in earth crust, which can neither be degraded nor destroyed (Zachariadis 2020). These toxic elements (irrigated by polluted water) congregated in food products like grains, fruits and vegetables can affect human health severely if consumed in high concentrations. The surveys claim that infants and children absorb these toxic elements five times more than adults (Samad *et al*. 2020). However nature has its own system for water recycling and recovery of contaminants but the population blast and rapid growth in industrialization have disturbed the routine natural distillation phenomena. Various chemical, physical and biological technologies are available to recover theses inorganic contaminants but nanoadsorbents play a significant role in the waste water treatment process by heavy metal removal (Chen *et al*. 2018, Punia *et al*. 2022a). Several methods like precipitation (Le *et al*. 2019), photocatalytic reduction (Liu *et al*. 2021) artificial membranes (Pham *et al*. 2021) and ion exchange (Smara *et al*. 2007) are developed to remediate waste water by removing the toxic metals from industrial effluents. These exclusive techniques are relatively incompetent and in nearly all cases they produce a large amount of sludge while handling of this toxic/non toxic waste is another challenge. Owing to properties like chemical stability and reusability, nanoferrite particles leave no such wastes in adsorption of heavy metals from contaminated water (Lata *et al*. 2015). Moreover, water management and treatment is more efficient through nanoadsorbents due to large surface area, excellent porosity and great adsorption capacity of the Ni-Zn ferrite nanoparticles (Rana *et al*. 2016, Reddy *et al*. 2016, Pathania *et al*. 2019, Punia *et al*. 2022b, Bharti *et al*. 2020). These ferrites can also be used for high frequency applications due to their suitable magnetic properties as materials with low hysteresis loss, high saturation magnetization and high electrical resistivity are best for the instruments like pulse transformers that operates on high frequencies (Thakur *et al*. 2011, Chahar *et al*. 2021 and Taneja *et al*. 2021). Some studies also reported that due to high adsorption capacity ferrites have shown excellent results in water purification process by removal of various heavy metals such as cadmium (Ahmed *et al*. 1998, Punia *et al*. 2021b), chromium (Hu *et al*. 2005), lead (Huang and Keller 2015), arsenic (Zhu *et al*. 2009), selenium (Ling *et al*. 2015) etc. from wastewater.

The current study aims towards the development of an adsorption process for cadmium and chromium removal from industrial waste water using Ni-Zn ferrite nano-particles as adsorbents. Several wet chemical as well as green synthesis methods are frequently used techniques to develop nanoparticles but citrate precursor method was used due to rapid growth of homogeneous nanoparticles

*Corresponding author, Professor,
E-mail: athakur@ggn.amity.edu
**Co-corresponding author, Professor,
E-mail: pthakur@ggn.amity.edu

ISSN: 2287-237X (Print), 2287-2388 (Online)

(Guptha *et al*. 2014, Mondal *et al*. 2016, Gokila *et al*. 2021). Already synthesized Ni-Zn nanoferrite materials with citrate precursor method were used to remove heavy metals from contaminated liquid samples. The results from XRD (X-ray Diffraction), FTIR (Fourier Transform Infrared) spectrometry and VSM (Vibrating Sample Magnetometer), with their detailed analysis, have already been reported (Punia *et al*. 2021a). Furthermore, the kinetic studies were done for the adsorption of Cd and Cr industrial wastewater using Lagergren's adsorption kinetic models. It is worth to mention here that no study has been reported till now for these heavy metal ions removal using Ni-Zn nanoferrites as adsorbents.

2. Materials and methods

2.1 Synthesis of adsorbents

The Ni-Zn ferrite nanoparticles were developed by the citrate precursor route using elements of analytical grade (Nickel Nitrate ($Ni(NO_3)_2 \cdot 6H_2O$) from Thomas Baker with 99% purity, Zinc Nitrate ($Zn(NO_3)_2 \cdot 6H_2O$) from Thomas Baker with 98% purity, Ferric Nitrate ($Fe(NO_3)3 \cdot 9H_2O$) from Fisher Scientific laboratory with 98% purity and citric acid ($C_6H_8O_7$) from Thomas Baker with 99.5% purity. The process involves the word citrate as a blend of citric acid and metal nitrates. So the aforementioned precursors were amalgamated into distilled water in a stoichiometric ratio. In essence, the mixture was heated with uninterrupted stirring on a magnetic stirrer at a temperature of about 80°C until absolute solvent vanishing that ended with a dry and dark brown solid. The solid outcome was then milled to fine particles using a agate mortar pestle and to end with sintered at a temperature of 700°C for 3 h in a muffle furnace (Bioport). Fig. 1 represents the detailed procedure followed to develop the series of Ni-Zn nanoferrites. Eq. (1) shows the chemical reaction taking place during the synthesis of $Ni_xZn_{1-x}Fe_2O_4$ (x = 0.2) nanoferrite sample.

$$(0.2)Ni(NO_3)_2 + (0.8)Zn(NO_3)_2 + 2\mathrm{Fe}(NO_3)_3 + (\frac{44}{27})C_6H_8O_7 \longrightarrow Ni_{0.2}Zn_{0.8}Fe_2O_4 + (\frac{88}{9})CO_2 + \left(\frac{176}{27}\right)H_2O + (\frac{8}{3})NO_2 + (\frac{8}{3})N_2 \quad (1)$$

2.2 Characterizations

A MiniFlex II benchtop (Rigaku) X-ray diffractometer (CuK_α radiation at λ = 1.5403 Å) was used to investigate structural properties of prepared samples with 2θ (angle between transmitted and reflected beam) ranging from 20° to 80° with a step size of 0.02°. Fourier transform infrared spectroscopy (FTIR) was performed on a Spectrum BX-II instrument with wavelength ranging from 400 cm^{-1} to 4000 cm^{-1} and with a resolution of 0.5 cm^{-1}. Raman spectrometer of Reinshaw (Invia II) with a resolution more than 1 cm^{-1} was used to affirm the structural studies of the Ni-Zn magnetic nanoferrites. The morphological studies were inspected via Jeol Scanning Electron Microscope (SEM) with EDS with a magnification of 27 Kx.

Fig. 1 Synthesis method to prepare powdered samples of highly magnetic Ni-Zn nanoferrites

The HRTEM instrument of TECNAI 200 kV (Fei, Electron Optics) was used to examine the nanostructure of the samples. Magnetic studies were examined with a Vibrating Sample Magnetometer (VSM) Microsense EV-9 under persuade of a high magnetic field of 10 kOe. Atomic absorption spectrometer (AAS) of Spectroquant Pharo 300 (Merck) was used to detect and evaluate heavy metal concentrations using identified heavy metal kit.

2.3 Adsorption experiments

To study the effect of contact time and Nickel doping on adsorption of Cd and Cr onto Ni-Zn nanoferrites, two different batch tests were run in sequence. At first, the nanoparticles of prepared $ZnFe_2O_4$ ferrite were used as adsorbents to remove heavy metals (Cd and Cr) from industrial wastewater to check the consequences of contact time on the rate of adsorption. Essentially, batch solutions were prepared with dilution (10 times) of 1 ml of the industrial wastewater using distilled water. Standardized Cd and Cr kits of Merck were employed to detect heavy metals. Initial concentrations (C_i) of Cd and Cr were found to be 0.989 mg/L and 1.28 mg/L respectively after dilution. The adsorbent dosage was 1 mg/25 mL and the adsorption of heavy metals was observed for a contact time of 2-10 min for all samples. The solution was then kept in a Rotary Flask Shaker (MICROSIL, INDIA) at room temperature. The pH of prepared solution was kept constant at 7.4. A tiny amount of this solution was tested after every 2 minutes to examine the amount of adsorbed heavy metal ions. Before undergoing AAS examination the samples were filtered through 125 mm filter papers.

Further, to ensure the influence of Ni-substitution on the adsorption rate of Cd and Cr another batch test was performed. All other parameters (adsorbent dose, pH and temperature) for this batch test were kept same as previous one except the initial concentrations of Cd and Cr, which were 2.15 mg/L and 2.35 mg/L respectively. As a consequence of the observations from the former batch test the contact times were kept fixed for Cd and Cr as 10 min. for all the prepared adsorbent nanoparticles. Equation 2 and 3 were used to determine the adsorption efficiency and percentage removal of heavy metals using synthesized nano-adsorbents.

$$Q_e = \frac{(C_i - C_f)V_s}{m} \quad (2)$$

$$R(\%) = \frac{(C_i - C_f)}{C_i} \times 100 \quad (3)$$

where, Q_e is quantity of adsorbed heavy metal ions per unit mass of adsorbents, C_i and C_f are initial and final concentrations respectively, m is mass of the nano-adsorbents, V_s is volume of solution used and R (%) is removal capacity of the adsorbent.

3. Results and discussion

3.1 Characterizations of nanoadsorbents

Fig. 2 shows the XRD patterns for $Ni_xZn_{1-x}Fe_2O_4$ (x = 0.0, 0.2, 0.4, 0.6, 0.8 and 1.0) series of samples. Structural properties of this series of samples have been studied using XRD data. Influence of nickel concentration on crystallite size (D), theoretical density (ρ_{th}), and specific surface area (*SSA*) of Ni-Zn nanoferrites was explored and calculated using the XRD data as shown in Table 1.

The average crystallite size of the samples was calculated with the help of Scherrer's equation:

$$D_{(hkl)} = 0.9\lambda/\beta\cos\theta \quad (4)$$

where, D was crystallite size, λ is wavelength of X-ray used, β is FWHM and θ is diffraction angle. The constant factor 0.9 is also known as shape factor (K) relates to 1D, 2D or 3D set of planes and have this value close to unity only applied to 1D set of planes. However the value of the shape factor may vary with the shape and size of the nano-crystallite for e.g. the value of K = 1.11 for spherical cubic lattices having 3D set of planes. The average crystallite size was found to vary in a range 24 nm-31 nm. The theoretical density was determined using following equation:

$$\rho_{th} = 8M/Na^3 \quad (5)$$

where, M is molecular weight of the nanomaterials, N is Avogadro's number and 'a' is the calculated lattice parameter. The specific surface area is one of the most important parameters for adsorption, exterior reactions and heterogeneous catalysis. The Sauter's formula was used to calculate the specific surface area of the nanoparticles depicted by Eq. (6):

$$SSA = \frac{6000}{\rho_{th} \times D} \quad (6)$$

Porosity (P) of all the samples is determined by the following formula,

$$P = \left(1 - \frac{\rho_{th}}{\rho_{exp}}\right) \times 100 \quad (7)$$

where, ρ_{exp} is experimental density or bulk density of prepared nanoferrites. Porosity of all the samples perceived to vary in a range 52% -56%, which is good enough to use as an adsorbent for heavy metal removal from industrial wastewater.

Raman spectroscopy is the best tool to find out the structure and structural disorder of the nanoferrites by the analysis of different vibrational modes in the Raman spectra. XRD confirmed the inverse spinel structure of the all the Ni-Zn nanoferrites and in inverse spinel structure the trivalent ions holds all the tetrahedral ions while octahedral sites are filled by divalent ions as well as remaining trivalent ions (Graves *et al*. 1988). The spinel structure has the Fd3m (O^7_h) and vibrational modes for spinel ferrites are

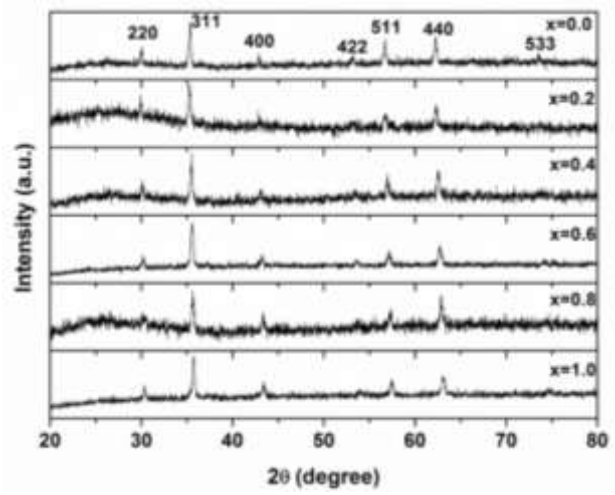

Fig. 2 XRD patterns of $Ni_xZn_{1-x}Fe_2O_4$ (x = 0.0, 0.2, 0.4, 0.6, 0.8 and 1.0) nanoferrites sintered at 700°C

Table 1 Effect of nickel concentration on structural parameters of prepared nanoadsorbents

Ni-concentration (x)	β(radians)	2θ	D(nm)	ρ_{th}(g/cm^3)	Specific surface area (*SSA*) cm^2/g
0.0	0.2864	35.33	31.32	5.358	35.75
0.2	0.3149	35.27	26.49	5.304	42.70
0.4	0.2337	35.47	24.70	5.363	45.29
0.6	0.3324	35.64	25.11	5.407	44.19
0.8	0.3301	35.56	25.29	5.340	44.42
1.0	0.3353	35.72	24.90	5.381	44.78

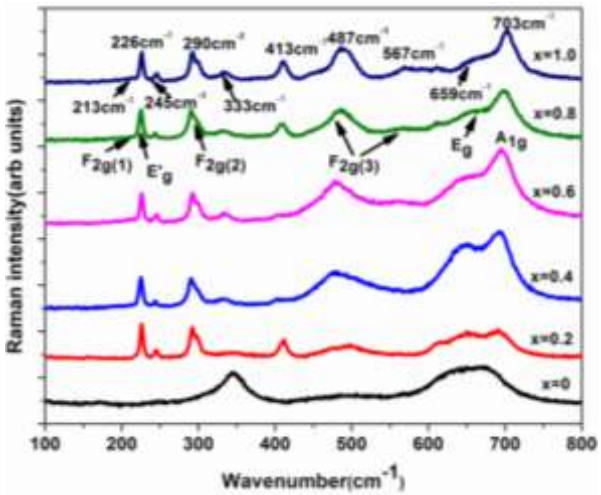

Fig. 3 Raman spectra of $Ni_xZn_{1-x}Fe_2O_4$ (x = 0.0, 0.2, 0.4, 0.6, 0.8 and 1.0) nanoferrites

given below.

$$A_{1g} + E_g + F_{1g} + 3F_{2g} + 2A_{2u} + 2E_u + 4F_{1u} + 2F_{2u} \quad (8)$$

where A_{1g}, E_g and F_{2g} are active Raman modes and F_{1u} is IR active mode while all others are silent modes. A broader spectrum was revealed for the $Ni_xZn_{1-x}Fe_2O_4$ (x = 0.0, 0.2, 0.4, 0.6, 0.8 and 1.0) series with high Zn concentrations while the peaks are very intense for Ni rich nanoferrites that can be seen from the Fig. 3 (Lazarević *et al*. 2012; Ehieromosele *et al*. 2015). This could be explained by the theory of cation distribution in inverse spinel ferrites that the Zn^{2+} ions with greater ionic radius than Ni^{2+} replace the Fe^{3+} ions with the increasing Zn concentration that causes lattice disorder. This lattice disorder due to the dislocation of Fe^{3+} ions leads to the broadening of the spectra. A_{1g} band ranging from 672-703 cm^{-1} shifting towards higher frequencies with increasing value of 'x' can be attributed to this cation exchange and ordering of octahedral sites (Singh *et al*. 2013). The frequency bands above 600 cm^{-1} correspond to the shifting of oxygen ions at tetrahedral sites and the vibrational modes in the lower frequency band indicate the vibrations of oxygen atom in octahedral sites (Kumbhar *et al*. 2015). E_g = 333-345 cm^{-1}, $F_{2g}(1)$ = 213 cm^{-1}, $F_{2g}(2)$ = 333-345 cm^{-1} and $F_{2g}(3)$ = 469-487 cm^{-1}, 567 cm^{-1} are other active Raman modes observed from the spectra. $F_{2g}(3)$ modes are shifting towards higher frequency bands while the E_g modes are moving towards lower frequencies (Massoudi *et al*. 2020).

Two supplementary shoulder peaks appeared in the spectra, one with the A_{1g} symmetry towards the lower frequency band and the other one is around 567 cm^{-1} which is accredited to the F_{2g} vibrational modes (Lahouli *et al*. 2019). One extra peak near the A_{1g} mode could be explained as the effect of cation distribution at both A and B sites while the other one could be due to the ions exchange at the B-sites only (Jadhav *et al*. 2017). The cation distribution on the lattice sites in the spinel ferrites could alter with synthesis process.

To obtain an accurate estimation of the microstructure and morphology of the nano-crystals, scanning electron microscopy has been performed. The SEM images of $Ni_xZn_{1-x}Fe_2O_4$ (x = 0.0, 0.2, 0.4, 0.6, 0.8 and 1.0) nanoparticles are shown in Fig. 4, which demonstrates that all the samples are in nano regime. All samples showed a tendency towards agglomeration can be due to electrostatic effects as well as an artifact of the drying of aqueous suspensions and to magnetic interaction arising among of nano- particles, revealing the formation of spherical and uniformly distributed nanoparticles. The grains are almost homogeneously distributed throughout the sample surface. The elemental analysis of all the prepared samples, measured using EDAX at room temperature, is shown in Fig. 5. The spectrum confirms the existence of all chemical elements Fe, Zn, Ni and O in the synthesized samples, which depicts that there was no loss of any integrated elements and no contamination during the sintering process. The result of EDAX predicted the required proportion of the constituents as well as the chemical purity of the samples, denoting a homogeneous chemical composition.

To confirm the formation of nanometric particles of Ni-Zn ferrite materials obtained via citrate precursor route,

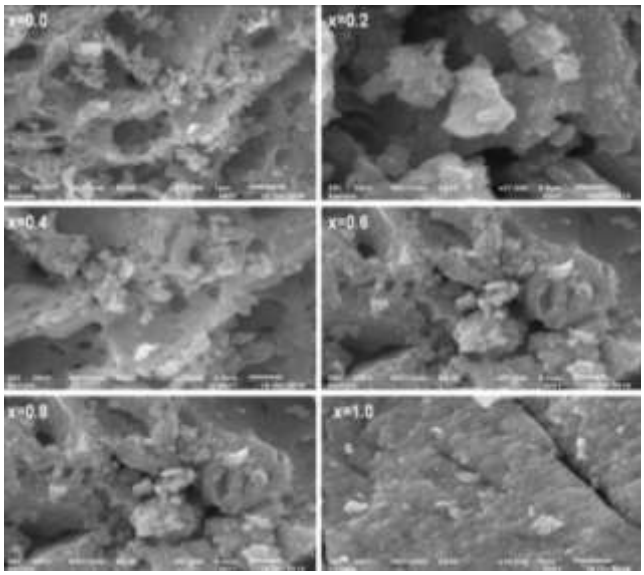

Fig. 4 SEM micrographs for $Ni_xZn_{1-x}Fe_2O_4$ (x = 0.0, 0.2, 0.4, 0.6, 0.8 and 1.0) series of samples

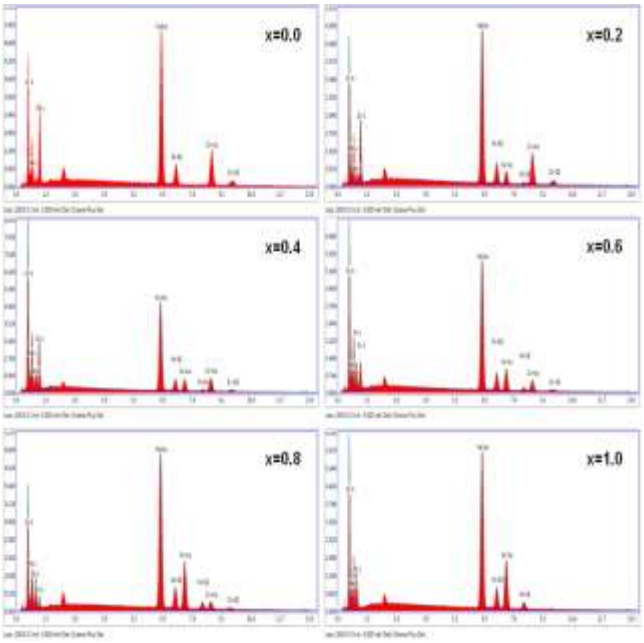

Fig. 5 EDAX spectra for $Ni_xZn_{1-x}Fe_2O_4$ (x = 0.0, 0.2, 0.4, 0.6, 0.8 and 1.0) nanomaterials

Transmission Electron Microscopes (TEM) investigations were performed for the samples $Ni_xZn_{1-x}Fe_2O_4$ (x = 0.2, 0.6, 0.8) nanoferrites by using Morgagni 268D (Fei Electron Optics). The TEM images are shown in Figs. 6(a)-6(c) for x = 0.2, 0.6 and 0.8, respectively. Uniform and homogenous nanoparticles with an average crystallite size of 10 nm can be noticed from TEM images.

3.2 Adsorption studies

3.2.1 Adsorption mechanism

The mechanism elucidating the adsorption of cadmium and chromium onto Ni-Zn nanoparticles was investigated using batch experiments and spectroscopic techniques. In

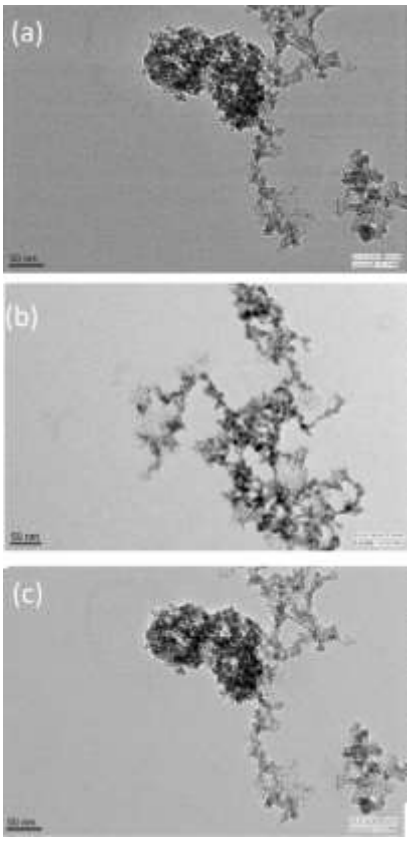

Fig. 6 TEM images of prepared $Ni_xZn_{1-x}Fe_2O_4$ with (a) x = 0.2, (b) x = 0.6, and (c) x= 0.8

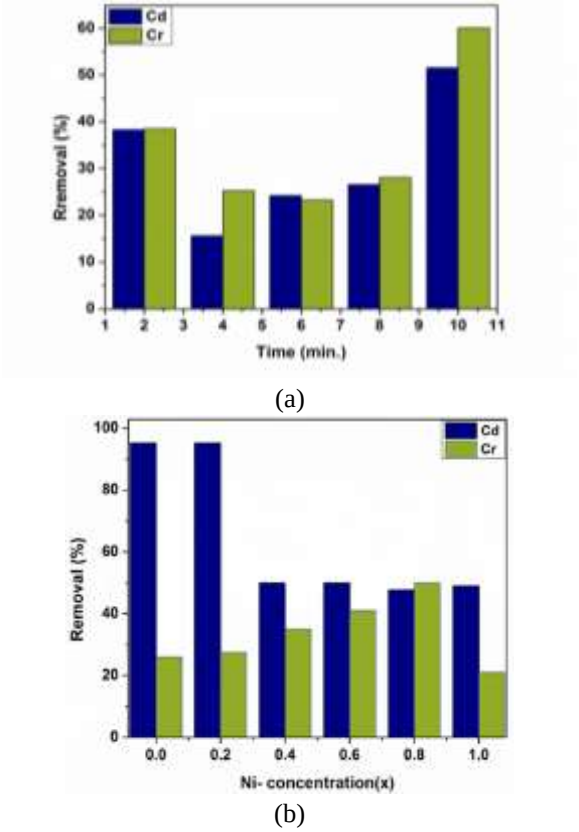

Fig. 7 Effect of (a) contact time on removal of cadmium and chromium onto $Ni_{0.2}Zn_{0.8}Fe_2O_4$ nanoparticles with contact time (2-10 min.), adsorbent dose (1 mg/25 ml), initial conc. (0.989 mg/L for Cd and (1.28mg/L for Cr), and pH (7.4) at room temperature and (b) dopant (nickel) concentration on removal of cadmium and chromium onto $Ni_xZn_{1-x}Fe_2O_4$ (x = 0.0, 0.2, 0.4, 0.6, 0.8 and 1.0) nano-particles; adsorbent dose (1 mg/25 ml); initial conc. (2.15 mg/L for Cd and 2.35 mg/L for Cr); t =10 min. and pH (7.4) at room temperature

order to confirm the occurrence of any chemical redox reaction throughout the adsorption process, the analysis of heavy metal ion concentration in the sample solution and nature of adsorbent's surface is essential. The cadmium and chromium ions dissipated into liquid were detected and evaluated using atomic adsorption spectrophotometer. According to previous studies, at lower pH values (<6) chromium exists in the form of $(Cr_2O_7)^-$ and $(HCrO_4)^-$ in the contaminated liquid sample and $(HCrO_4)^-$ dominates the earlier ones (Sezgin *et al*. 2015, Singh *et al*. 2017). Though at pH above 6 chromium is found in the form of $(CrO_4)^{2-}$ and $(Cr_2O_7)^{2-}$. Following are the equilibrium relations for chromium:

$$HCr_2O_7^- \leftrightarrow Cr_2O_7^- + H^+ \quad (9)$$

$$Cr_2O_7^{2-} + H_2O \leftrightarrow 2HCrO_4^- \quad (10)$$

$$HCrO_4^- \leftrightarrow CrO_4^{2-} + H^+ \quad (11)$$

$$HCrO_4^- \leftrightarrow HCrO_4^- + H^+ \quad (12)$$

However at higher pH values adsorption rate slows down but with the Ni-Zn nanoferrites high adsorption rates up to 95.25% for Cd were achieved even at high pH value (7.4) using $ZnFe_2O_4$ nanoparticles within 2 minutes. Further, negative charge emerges on the surface of adsorbent used in contaminated sample at high pH. This results to the attraction force between cadmium ions and active sites of used adsorbents. Cadmium removal may undergo declining because of the cadmium hydroxide precipitates. Beyond physisorption (physical adsorption), following chemical reactions may also occur during cadmium adsorption process:

$$2(NZNPs)\text{-}H + Cd \leftrightarrow (NZNPs)_2Cd + 2H^+ \quad (13)$$

$$(NZNPs)\text{-}H + Cd(OH)+ \leftrightarrow (NZNPs)\text{-}Cd(OH) + H^+ \quad (14)$$

The occurrence of physisorption and chemisorption can be confirmed via kinetic and isothermal adsorption studies. It was observed that more than 60% of cadmium content found to be adsorbed using 1mg of magnetic $NiFe_2O_4$ nanoadsorbents after a contact time of 10 min. The used adsorbent nanoparticles were recovered from the sample solution after adsorption using magnetic field and filtration. The adsorbed heavy metals can be regenerated via various techniques and reused for further adsorption experiments.

3.2.2 Effect of contact time and dopant concentration

In order to establish adsorption kinetics the effect of contact time on adsorption capacity is a crucial parameter. The consequences of increasing contact time from 2 to 10

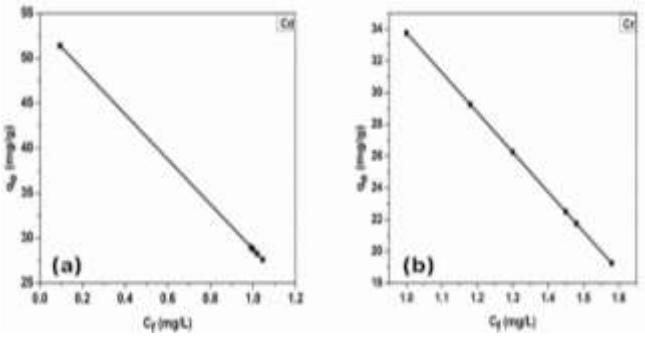

Fig. 8 Plots of final concentrations (C_f) versus adsorption efficiency (q_e) of (a) cadmium (Cd) and (b) chromium (Cr) using $Ni_xZn_{1-x}Fe2O4$ (x = 0.0, 0.2, 0.4, 0.6, 0.8 and 1.0) as adsorbents. Dose: 1mg/25mL, C_o (Cd): 2.15 mg/L, C_o (Cr): 2.35 mg/L, pH: 7.4, T: 25 ± 1°C

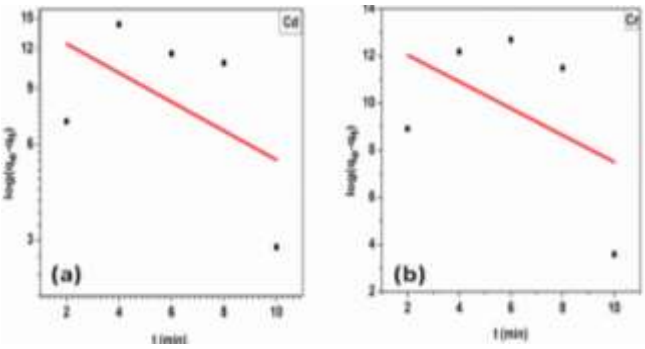

Fig. 9 Pseudo-first-order models for removal of (a) cadmium (Cd) and (b) chromium (Cr) using $Ni_{0.2}Zn_{0.8}Fe_2O_4$ nanoparticles; Dose: 1 mg/25 mL; C_i (Cd): 0.989 mg/L; C_i (Cr): 1.28 mg/L; pH: 6.0; T: 25 ± 1°C

min. on adsorption of cadmium and chromium onto Ni-Zn nanoadsorbents with pH value 7.4 at room temperature are depicted in Fig. 7(a) The fast adsorption of cadmium and chromium onto prepared ferrite nanoparticles might be due to the outer surface adsorption instead of the microporous adsorption route. Almost all the adsorption sites or active sites for heavy metal ions in Ni-Zn nanoparticles exists on the external surface, which results in rapid adsorption of cadmium and chromium. As clearly elucidated by the Fig. 5, number of adsorbed heavy metal ions decreased initially from 38.2% to 15.6% for cadmium and from 38.6% to 25.2% for chromium. Negative charge with an increasingly overriding (≡Fe–O–4) entities, emerged on both the contaminant ions as well as exterior of nanoadsorbents for pH values beyond 7 (Guerrero *et al*. 2021). This fact resulted in enhancement of mutual electrostatic repulsion between both the species and hence the rapid decrease in ion adsorption was detected (Li *et al*. 2013). But due to the smaller particle size and large surface area with great number of active sites the uptake of cadmium and chromium ions increased further from 15.6% to 51.5% and from 25.2% to 60% respectively. The adsorption equilibrium was achieved after 10 min. for both the heavy metal ions.

Fig. 7(b) shows the effect of dopant (nickel) concentration on cadmium and chromium uptake from industrial wastewater using Ni-Zn nanoferrites. The removal percentage of cadmium (~95%) is maximum for $Ni_xZn_{1-x}Fe_2O_4$ (x = 0.0 and 0.2) while maximum uptake of chromium (50%) was detected using the $Ni_xZn_{1-x}Fe_2O_4$ (x = 0.8). Minimum removal of Cadmium (47.7%) and chromium (21%) was achieved by $Ni_xZn_{1-x}Fe_2O_4$ (x = 0.8) and $Ni_xZn_{1-x}Fe_2O_4$ (x = 1.0) respectively. The adsorption of heavy metal ions haven't shown any regular decrease or increase that may be attributed to many parameters like porosity, specific surface area and magnetic behavior of the individual adsorbents. It can also be ascribed to the no. of active site present on the external surface of nanoparticles. Furthermore, the presence of other contaminants may also affect the adsorption of cadmium and chromium on active sites (Chen *et al*. 2021). It was determined from this batch test that the prepared nanoferrites via citrate precursor route are suitable enough for effective adsorption of cadmium and chromium ions from contaminated water. Figs. 8(a) and 8(b) shows the linear relation between final concentrations (C_f) and adsorption efficiencies (q_e) of Cd and Cr respectively. The adsorption efficiency (q_e) for Cd was observed to vary in a range 27.6 mg/g -51.4 mg/g for varying Ni-concentration in prepared nanoadsorbents while for Cr the value of q_e lied in a range 19.25 mg/g -33.75 mg/g at room temperature. Due to Considerable adsorption capacities, synthesized nanoadsorbents depicted suitable candidature for Cd and Cr removal from aquatic solutions.

3.2.3 Adsorption kinetics

The popular pseudo-first-order and pseudo-second-order kinetic models developed in 1898 by Lagergren were used to determine the adsorption kinetics for cadmium and chromium. The following equation demonstrates the linear form of pseudo- first-order kinetic model equation:

$$\ln(q_e - q_t) = lnq_e - k_1 t \qquad (15)$$

where, q_e is the adsorption efficiency at equilibrium; q_t is the adsorption efficiency of target heavy metal ions at time t (min.); k1 is the rate constant of pseudo-first-order kinetic model; t is the contact time (min.). The equilibrium adsorption efficiency qe and the adsorption rate constant k1 can be determined from the slopes and intercepts of plots of log ($q_e - q_t$) vs. t respectively given in Fig. 9.

Fig. 10 represents the plots of pseudo-second-order kinetic model for cadmium and chromium adsorption data. The linear expression of the pseudo-second-order kinetic model is given as Eq. (16):

$$\frac{t}{q_t} = \frac{1}{k_2 {q_e}^2} + \frac{t}{q_e} \qquad (16)$$

where, k_2 (g/mg min) is the rate constant of pseudo- second-order kinetic h can be determined with the slope of plots of t/q_t vs. t while the intercept of the plot gives adsorption efficiency at equilibrium. The correlation of the calculated adsorption efficiencies from the experimental adsorption data with the theoretical values along with the correlation factor (R^2) confirms the best fit of the data with either one of the kinetic models.

The adsorption mechanism taking place during the It can be seen clearly through Figs. 9 and 10 that the adsorption data deemed to fit to pseudo second order kinetic model. The correlation factor R^2 has higher values for PSO

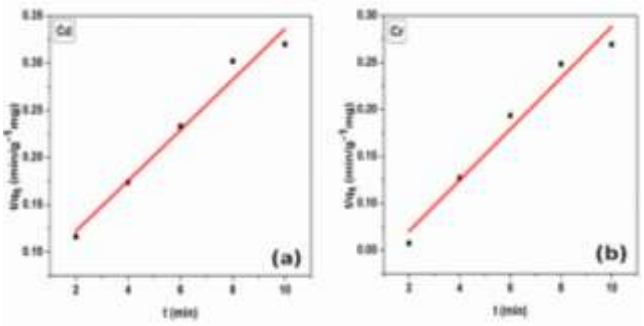

Fig. 10 Pseudo-second-order model for removal of (a) cadmium and (b) chromium using 1 mg of $Ni_{0.2}Zn_{0.8}Fe_2O_4$ nanoparticles as adsorbents; Dose: 1 mg/25 mL; C_i (Cd): 0.989 mg/L, C_i (Cr): 1.28 mg/L; pH: 6.0; T: 25 ± 1°C

Table 2 Kinetic parameters for adsorption of Cd and Cr onto Ni-Zn nanoferrite adsorbents at temperature 25°C

Kinetic model	Cd	Cr
q_e *(mg/g)(exp)*	34.5	40.12
Pseudo first order		
k_1 *(min^{-1})(×10^{-2})*	4.57	56.75
q_e *(mg/g)*	3.22	35.81
R^2	0.02489	0.02805
Pseudo second order		
k_2 *(g/ min.mg) (×10^{-2})*	1.1	4.7
q_e *(mg/g)*	37.35	36.71
R^2	0.96868	0.95907

data plots than PFO as shown in Table 2. Additionally, the experimental values of adsorption efficiencies (q_e) for Cd (34.5 mg/g) and Cr (40.12 mg/g) are more relevant to the calculated values of adsorption efficiencies for Cd (37.35 mg/g) and Cr (36.71 mg/g) from PFO kinetic model. It can be inferred that the heavy metal ions were adsorbed physically on the outer surface of the adsorbent nanoparticles.

4. Conclusions

Adsorption experiments were performed to remove Cd and Cr ions from industrial waste water with optimum dosages.

• SEM and EDAX studies confirmed the formation of spinel nanoferrites with high purity

• Raman spectra exposed the structural disorder due to this cation exchange and ordering of octahedral sites represented by the shifting of A_{1g} band ranging from 672 cm^{-1}-703 cm^{-1} with decreasing Ni-concentration.

• The present study revealed that Ni-Zn nanoferrites with different compositions are efficient adsorbents for Cd and Cr removal from industrial wastewater. The optimum value for contact time was recorded as 10 min. for both the heavy metal ions at pH∼7 with a fix adsorbent dose of 1mg in 25 mL of diluted contaminated water.

• Kinetic studies confirmed the best fit of adsorption data to pseudo second order kinetic model. The observed R^2 values for PSO data plots were closer to 1.0 for both Cd and Cr.

• Moreover, the calculated values of adsorption efficiencies (q_e) from PSO model for both heavy metal contaminants were found more consistent with the experimental values. This fact depicted the chemical adsorption of the heavy metals on the outer surface of nanoparticles and no chemical reactions were observed among adsorbates and adsorbents. The metal loaded adsorbents can be regenerated using acids and other chemical reagents via desorption process with very low efficiency losses. This reflects the chemical stability of nanoferrites prepared via citrate precursor method as adsorbents.

Acknowledgments

The author(s) would like to acknowledge the support provided under the DST-FIST Grant No. SR/FST/PS-I/2018/48 of Govt. of India. Authors also wish to acknowledge Gurujal, an initiative with district administration Gurugram for financial assistance vide project No176 Gurujal dated September 10, 2019, Amity Incubation grant from The Ministry of Electronics and Information Technology: (Meity) under Technology Incubation and Development of Entrepreneurs (TIDE 2.0) program and the startup nanoLatticeX

References

Ahmed, S., Chughtai, S., Keane M.A. (1998), "The removal of cadmium and lead from aqueous solution by ion exchange with Na-Y zeolite", *Sep. Purif. Technol.* **13**, 57-64. https://doi.org/10.1016/S1383-5866(97)00063-4.

Bharti, M.K., Gupta, S., Chalia, S., Garg, I., Thakur, P. and Thakur, A. (2020), "Potential of magnetic nanoferrites in removal of heavy metals from contaminated water : Mini review", *J. Supercond. Nov. Magn.*, **33**, 3651-3665. https://doi.org/10.1007/s10948-020-05657-1.

Chahar, D., Taneja, S., Bisht, S., Kesarwani, S., Thakur, P., Thakur, A. and Sharma, P.B. (2021), "Photocatalytic activity of cobalt substituted zinc ferrite for the degradation of methylene blue dye under visible light irradiation", *J. Alloys Compd.*, **851**, 156878 1-9. https://doi.org/10.1016/j.jallcom.2020.156878.

Chen, F., Guo, S., Wang, Y., Ma, L., Li, B., Song, Z., Huang, L. and Zhang, W. (2021), "Concurrent adsorption and reduction of chromium(VI) to chromium(III) using nitrogen-doped porous carbon adsorbent derived from loofah sponge", *Front. Environ. Sci. Eng.*, **16**(57). https://doi.org/10.1007/s11783-021-1491-6.

Chen, J., Wang, N., Liu, Y., Zhu, J.,Feng, J. and Yan, W. (2018), "Synergetic effect in a self-doping polyaniline/TiO2 composite for selective adsorption of heavy metal ions", *Synth. Met.*, **245**, 32-41. https://doi.org/10.1016/j.synthmet.2018.08.006.

Ehi-eromosele, C., Ita, B., Iweala, E. and Iweala S.A. (2015), "Magneto-structural properties of Ni - Zn nanoferrites synthesized by the low-temperature auto-combustion method", *Bull. Mater. Sci.*, **38**, 1-8. https://doi.org/10.1007/s12034-015-1038-1.

Gokila, V., Perarasu, V.T. and Rufina, R.D.J. (2021), "Qualitative comparison of chemical and green synthesized Fe_3O_4

nanoparticles", *Adv. Nano Res.*, **10**(1), 71-76. https://doi.org/10.12989/ANR.2021.10.1.071.

Graves, P.R., Johnston, C. and Campaniello, J.J. (1988), "Raman scattering in spinel structure ferrites", *Mater. Res. Bull.*, **23**, 1651-1660. https://doi.org/10.1016/0025-5408(88)90255-3.

Guerrero, A.V., Martínez, C.R, Alfaro-Cuevas-villanueva, R., Rivera-Muñoz, E.M. and Huirache-Acuña, R. (2021), "CD(II) and PB(II) adsorption using a composite obtained from moringa oleifera lam. cellulose nanofibrils impregnated with iron nanoparticles", *Water (Switzerland)*, **13**, https://doi.org/10.3390/w13010089.

Guptha, K.V. and Nesaraj, A.S. (2014), "Solvothermal synthesis and characterization of silver nanoparticles", *Adv. Nano Res.*, **2**(3), 147-155. https://doi.org/10.12989/ANR.2014.2.3.147.

Hu, J., Chen, G. and Lo Ã I.M.C. (2005), "Removal and recovery of Cr (VI) from wastewater by maghemite nanoparticles", *Water Res.*, **39**(18), 4528-4536. https://doi.org/10.1016/j.watres.2005.05.051.

Huang, Y. and Keller, A.A. (2015), "EDTA functionalized magnetic nanoparticle sorbents for cadmium and lead contaminated water treatment", *Water. Res.* **80**, 159-168. https://doi.org/10.1016/j.watres.2015.05.011.

Jadhav, J., Biswas, S., Yadav, A.K., Jha, S.N. and Bhattacharya, D. (2017), "Structural and magnetic properties of nanocrystalline Ni[sbnd]Zn ferrites: In the context of cationic distribution", *J. Alloys Compd.*, **696**, 28-41. https://doi.org/10.1016/j.jallcom.2016.11.163.

Kumbhar, S.S., Mahadik, M.A., Mohite, V.S., Hunge, Y.M., rajpure, K.Y., and Bhosale, C.H. (2015), "Effect of Ni content on the structural, morphological and magnetic properties of spray deposited Ni-Zn ferrite thin films", *Mater. Res. Bull.*, **67**, 47-54. https://doi.org/10.1016/j.materresbull.2015.02.056.

Lahouli, R., Massoudi, J., Smari, M., Rahmouni, H., Khirouni, K., Dhahri, E. and Bessais, L.(2019), "Investigation of annealing effects on the physical properties of $Ni_{0.6}Zn_{0.4}Fe_{1.5}Al_{0.5}O_4$ ferrite", *RSC Adv.*, **9**, 19949-19964. https://doi.org/10.1039/c9ra02238d.

Lata, S., Singh P.K. and Samadder, S.R. (2015), "Regeneration of adsorbents and recovery of heavy metals: A review", *Int. J. Environ. Sci. Technol.*, **12**, 1461-1478. https://doi.org/10.1007/s13762-014-0714-9.

Lazarević, Z.Ž., Jovalekić, Č., Milutinović, A., Roṁević, M.J. and Romčević, N.Ž. (2012), "Preparation and characterization of nano ferrites", *Acta Phys. Pol. A.*, **121**, 682-686. https://doi.org/10.12693/APhysPolA.121.682.

Le, A.T., Pung, S.Y., Sreekantan, S., Matsuda, A. and Huynh, D.P. (2019), "Mechanisms of removal of heavy metal ions by ZnO particles", *Heliyon*, **5**, 1-27. https://doi.org/10.1016/j.heliyon.2019.e01440.

Li, Y., Ma, H., Ren, B. and Li, T. (2013), "Simultaneous adsorption and degradation of Cr(VI) and Cd(II) ions from aqueous solution by silica-coated Fe0 nanoparticles", *J. Anal. Methods Chem.*, **2013**, 1-8 https://doi.org/10.1155/2013/649503.

Ling, L., Pan, B., Zhang, W. xian (2015), "Removal of selenium from water with nanoscale zero-valent iron: Mechanisms of intraparticle reduction of Se(IV)", *Water. Res.*, **71**, 274-281. https://doi.org/10.1016/j.watres.2015.01.002.

Liu, D., Wang, Y., Xu, X., Xiang, Y., Yang, Z. and Wang, P. (2021), "Highly efficient photocatalytic Cr(VI) reduction by lead molybdate wrapped with D-A conjugated polymer under visible light", *Catalysts* **11**, 1-15. https://doi.org/10.3390/catal11010106.

Massoudi, J., Smari, M., Nouri, K., Dhahri E., Khirouni, K., Bertaina, S., Bessais, L. and Hlil, E.K. (2020), "Magnetic and spectroscopic properties of Ni-Zn-Al ferrite spinel: From the nanoscale to microscale", *RSC Adv.*, **10**, 34556-34580. https://doi.org/10.1039/d0ra05522k.

Mondal, S., Dey, A. and Pal, U. (2016). "Low temperature wet-chemical synthesis of spherical hydroxyapatite nanoparticles and their in situ cytotoxicity study", *Adv. Nano Res.*, **4**(4), 295-307. https://doi.org/10.12989/ANR.2016.4.4.295.

Pathania, A., Thakur, P., Trukhanov, A. V., Trunkhanov, S.V., Panina, L.V., Luders, U. and Tahkur, A. (2019), "Development of tungsten doped Ni-Zn nano-ferrites with fast response and recovery time for hydrogen gas sensing application", *Results Phys.*, **15**, 102531. https://doi.org/10.1016/j.rinp.2019.102531.

Pham, M.T., Nishihama, S. and Yoshizuka, K. (2021), "Removal of chromium from water environment by forward osmosis system", *MATEC Web Conf.*, **333**, 1-5. https://doi.org/10.1051/matecconf/202133304007.

Punia, P., Dhar, R., Ravelo, B., Trukhanov, A.V., Panina, L.V., Thakur, P. and Thakur, A. (2021a), "Microstructural, optical and magnetic study of Ni - Zn nanoferrites", *J. Supercond. Nov. Magn.*, **34**(8), 2131-2140. https://doi.org/10.1007/s10948-021-05967-y.

Punia, P., Bharti, M.K., Chalia, S.,Dhar, R., Ravelo, B., Thakur, P. and Thakur, A. (2021b), "Recent advances in synthesis, charateriztion and applications of nanoparticles for contaminated water treatment - a review", *Ceram. Int.*, **47**(2), 1526-1550. https://doi.org/10.1016/j.ceramint.2020.09.050.

Punia, P., Bharti, M.K., Dhar, R., Thakur, P. and Thakur, A. (2022a), "Recent advances in detection and removal of heavy metals from contaminated water", *ChemBioEng. Rev.*, **9**, 1-20. https://doi.org/10.1002/cben.202100053.

Punia, P., Aggarwal R.K., Kumar, R., Dhar, R., Thakur, P. and Thakur, A. (2022b), "Adsorption of Cd and Cr ions from industrial wastewater using Ca doped Ni-Zn nanoferrites: Synthesis, characterization and adsorption iaotherm analysis", *Ceram. Int.*, In Press. https://doi.org/10.1016/j.ceramint.2022.02.234.

Rana, K., Thakur, P., Tomar, M., Gupta, V. and Thakur, A. (2016), "Structural and magnetic properties of Ni-Zn doped BaM nanocomposite via citrate precursor method", *AIP Conference Proceedings*, **1731**, 1-4. https://doi.org/10.1063/1.4947806.

Reddy, D., Kumar, H. and Yun, Y.S. (2016), "Spinel ferrite magnetic adsorbents: Alternative future materials for water purification", *Coord. Chem. Rev.*, **315**, 90-111. https://doi.org/10.1016/j.ccr.2016.01.012.

Samad, A., Din M.I. and Ahmed, M. (2020), "Studies on batch adsorptive removal of cadmium and nickel from synthetic waste water using silty clay originated from Balochistan-Pakistan", *Chinese. J. Chem. Eng.*, **28**, 1171-1176. https://doi.org/10.1016/j.cjche.2019.12.016.

Sezgin, N., Yalçın, A. and Köseoğlu, Y. (2015), "$MnFe_2O_4$ nano nano spinels as potential sorbent for adsorption of chromium from industrial wastewater", *Desalin. Water Treat.*, **57**(35), 16496-16506. https://doi.org/10.1080/19443994.2015.1088808.

Singh, J.P., Dixit, G., Srivastava, R.C., Agrawal, H.M. and Kumar, R. (2013), "Raman and Fourier-transform infrared spectroscopic study of nanosized zinc ferrite irradiated with 200 MeV Ag^{15+} beam", *J. Alloys Compd.*, **551**, 370-375. https://doi.org/10.1016/j.jallcom.2012.10.006.

Singh, K., Renu, N.A. and Agarwal, M. (2017), "Methodologies for removal of heavy metal ions from wastewater: An overview", *Interdiscip. Environ. Rev.*, **18**, 124. https://doi.org/10.1504/ier.2017.10008828.

Smara, A., Delimi, R., Chainet, E. and Sandeaux, J. (2007), "Removal of heavy metals from diluted mixtures by a hybrid ion-exchange/electrodialysis process", *Sep. Purif. Technol.*, **57**,103-110. https://doi.org/10.1016/j.seppur.2007.03.012.

Taneja, S., Chahar, D., Thakur, P. and Thakur, A. (2021), "Influence of bismuth doping on structural, electrical and dielectric properties of Ni-Zn nanoferrites", *J. Alloys Compd.*,

859, 157760. https://doi.org/10.1016/j.jallcom.2020.157760.
Thakur, A., Thakur, P. and Hsu, J. (2011), "Enhancement in dielectric and magnetic properties of In3+ substituted ni-zn nano-ferrites by coprecipitation method", *IEEE T. Magn.*, **47**, 4336-4339. https://doi.org/10.1109/TMAG.2011.2156394.
Zachariadis, N.M. and G.A. (2020), "Development and application of an icp-aes method for the determination of nutrient and toxic elements in savory snack products after autoclave dissolution", *Separations*, **66**(7), https://doi.org/10.3390/separations7040066.
Zhu, H., Jia, Y., Wu, X. and Wang, H. (2009), "Removal of arsenic from water by supported nano zero-valent iron on activated carbon", *J. Hazard Mater.*, **172**, 1591-1596. https://doi.org/10.1016/j.jhazmat.2009.08.031.

SR